Local-moment and itinerant antiferromagnetism in the heavy-fermion system Ce(Cu$_{1-x}$Ni$_x$)$_2$Ge$_2$

A. Loidl[1,2], A. Krimmel[2,3], K. Knorr[2], G. Sparn[1], M. Lang[1], C. Geibel[1], S. Horn[1], A. Grauel[1], F. Steglich[1], B. Welslau[1], N. Grewe[1], H. Nakotte[4], F. R. de Boer[4], and A. P. Murani[3]

[1]Institut für Festkörperphysik, TH Darmstadt, W-6100 Darmstadt, Germany
[2]Institut für Physik, Johannes-Gutenberg-Universität Mainz, W-6500 Mainz, Germany
[3]Institut Laue-Langevin, F-38042 Grenoble, France
[4]Natuurkundig Laboratorium, Universiteit van Amsterdam, NL-1018 XE Amsterdam, The Netherlands

Abstract. Elastic and inelastic neutron-scattering studies on the system Ce(Cu$_{1-x}$Ni$_x$)$_2$Ge$_2$ are reported. These measurements are complemented by measurements of the magnetic susceptibility, high-field magnetization, heat capacity, thermal expansion, electrical resistivity and thermopower. The results reveal an interesting T-x phase diagram consisting of two different antiferromagnetic phases for $x < 0.2$ and $0.2 < x < 0.75$, respectively, and a heavy-Fermi-liquid regime at higher Ni concentrations. The experimental results are interpreted in terms of an alloying-induced transition from local-moment to itinerant heavy-fermion magnetism. Fingerprints of this latter phase are a strongly reduced ordered moment and a short incommensurate ordering wave vector, in accord with theoretical predictions. A surprisingly good agreement between theory and experiment is found for $x > 0.5$. Further experimental evidence for different types of antiferromagnetic ordering derives from a line-shape analysis of the quasielastic neutron-scattering intensity, from magnetization and thermopower experiments.

1 Introduction

Within the past decade heavy-fermion (HF) compounds, i.e. some $4f$- and $5f$-intermetallics, have been studied intensively in order to explore the physics of highly correlated electron systems [1]. In particular, the tetragonal ThCr$_2$Si$_2$ homologs provide a rich variety of materials that allow both, to verify basic concepts in HF physics and to investigate prototypical HF ground states. While lacking direct f-wave-function overlap, these compounds exhibit a distinct f-ligand hybridization which, along with strong many-body renormalizations below the so-called "Kondo-lattice temperature" T^*, are effective in forming heavy-mass quasiparticles. The exciting ground state properties, in particular superconductivity and lately a variety of new magnetic phenomena, have led to new concepts and are still intensely debated. The possibility of "heavy-fermion band magnetism" (HFBM), as to be distinguished from the more conventional local-moment magnetism (LMM) often found in $4f/5f$-compounds, has been introduced as theoretical concept [2, 3], which soon met experimental evidence [4]. It turned out, in fact, to be a

valuable tool in understanding the diverse properties of a large class of heavy-fermion materials at low temperatures [5].

The present investigation is devoted to the magnetic phase diagram of the quasibinary system $Ce(Cu_{1-x}Ni_x)_2Ge_2$. Whereas $CeCu_2Ge_2$ is a local-moment-type of antiferromagnet ($T_{N1} = 4.1$ K [6], $\mu_S \simeq 0.74\,\mu_B$ [7], $T^* \simeq 8 \pm 2$ K, $T_{RKKY} \simeq 7$ K [7]), $CeNi_2Ge_2$ belongs to the class of non-magnetic heavy-Fermi-liquid systems ($\gamma \simeq 0.4$ J/K^2 mole, $T^* \simeq 30$ K [8]). The mixed crystals have been investigated by heat capacity, thermal expansion, resistivity, thermopower, DC susceptibility and magnetization experiments [9, some preliminary results are given in Ref. 4]. As expected, Ni substitution causes a strong depression of $T_{N1}(x)$ which extrapolates to zero near $x = 0.2$. Fully unexpected, however, a second type of antiferromagnetic ordering develops at higher Ni concentrations below $T_{N2}(x)$. As we shall see below, this new antiferromagnetic state exhibits the signatures of HFBM, at least for Ni concentrations $x > 0.5$.

2 Theory

The competition between LMM and a Fermi-liquid ground state of heavy quasiparticles in Kondo lattices has traditionally been understood via a mutually destructive formation of different types of correlations, local singlet-binding and non-local alignment of localized existing moments [10]. Correspondingly, two energy scales as characteristic for the respective energy gain at $T = 0$ K, $k_B T_K \sim \exp(-1/g)$ and $k_B T_{RKKY} \sim g^2$ ($g = N_F J$, being the dimensionless effective exchange coupling constant between local moments and conduction electrons with density of state N_F at the Fermi level) have been compared to decide on the nature of the ground state. In the "deep" Kondo-regime, characterized by $g \ll 1$, clearly RKKY-magnetism is dominant. Heavy-fermion systems typically are characterized by a larger value of g, but are still far apart from the intermediate valence regime $g \sim 1$. Theoretical investigations [3, 11] point to a more subtle physical picture although concepts developed for the deep Kondo regime still are useful: Compensation of moments can proceed further, involving frozen-in short-range antiferromagnetic correlations. In this way a coherent heavy-Fermi-liquid state is formed at low temperatures, which is characterized by a new quasi-local energy scale T^* replacing T_K and by new effective interactions between quasiparticles. The dynamics of these new degrees of freedom involves generally small renormalized magnetic moments tied to heavy but itinerant single-particle excitations. The picture advocated here has found support, recently, by other studies of the low temperature states of Kondo-lattices, which were based on different approaches. In Ref. 12a perturbational treatment of the susceptibility of the lattice was combined with phenomenological arguments to derive similar conclusions; the particular emphasis on the dual nature of local f-electron-degrees of freedom was elaborated on in Ref. 13. Even within the variational Gutzwiller approach, which formerly predicted a universal instability of the Kondo lattice towards a magnetic state of RKKY type, now a wide region with a non-magnetic phase is obtained by using improved correlated wave functions [14].

An appropriate treatment of the whole temperature- and possibly also magnetic-field-dependent scenario [11] can be based on the LNCA version of perturbation-theory [2], which gives for the wave-vector- and frequency-dependent magnetic susceptibility:

$$\chi(\mathbf{q}, i\nu) = [\chi_0(i\nu)^{-1} - K(\mathbf{q}, i\nu)]^{-1} \tag{1}$$

The quasi-local susceptibility χ_0, describing moment compensation on a temperature scale T^*, is modified via local and non-local quasiparticle interactions contributing to the function K. This correction term embodies virtual excitations with high energies, which may be characterized as leading to RKKY-type interactions between largely unrenormalized moments, and low-energy processes which are subject to the strong renormalizations mentioned above. When approaching the heavy-Fermi-liquid state, by decreasing the temperature or increasing T^* as a result of pressure or alloying, the latter contributions can become dominant as a result of increased spectral weight and small excitation energies [3]. HFBM, as resulting from such an increased value of K at low temperatures $T < T^*$ and a corresponding instability $\chi_0(o)$ $K(\mathbf{q}_c, 0) \rightarrow 1$ in the susceptibility of Eq. (1) should typically involve (i) reduced moments and (ii) small critical wavevectors $\mathbf{q}_c$ as characteristic for hybridization gaps in the quasiparticle band structure. The latter may compete with, or completely replace the $2k_F$-modes with modulations typically on the scale of one lattice spacing which indicate RKKY-correlations. In the following we will give clear evidence for such a behavior in the $Ce(Cu_{1-x}Ni_x)_2Ge_2$-system.

3 Experimental details and results

This section is mainly devoted to unraveling the types of magnetic order that develop in $Ce(Cu_{1-x}Ni_x)_2Ge_2$. First, we present results of bulk and neutron scattering measurements that have been used to construct the concentration dependences of the Kondo-lattice temperature $T^*(x)$ as well as of the magnetic ordering temperatures $T_{N1}(x)$ and $T_{N2}(x)$, see Figs. 1 and 2. Additional emphasis will be put on the occurrence of two subsequent transitions in samples with Ni concentrations $0 < x \leq 0.3$, cf. hatched area in Fig. 2.
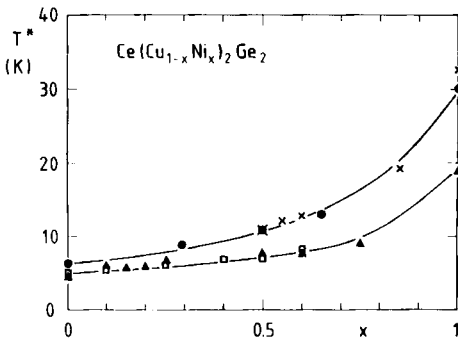

Fig. 1 "Kondo-lattice" temperature T^* vs x for $Ce(Cu_{1-x}Ni_x)_2Ge_2$ obtained from residual quasielastic magnetic line width ($\bullet$) as well as from maxima in the temperature dependences of the thermopower (scaled by factor 1.54, $\times$), thermal expansion ($\blacktriangle$) and electrical resistivity (scaled by factor 1.25, $\square$).
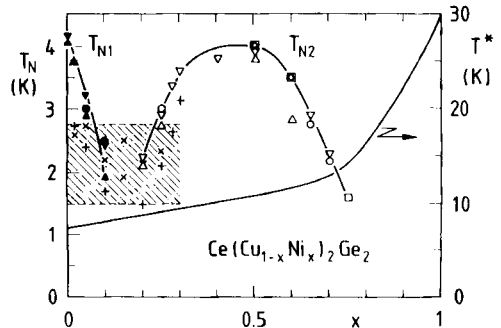
Fig. 2 T vs x phase diagram for $Ce(Cu_{1-x}Ni_x)_2Ge_2$. Left scale: Néel temperatures $T_{N1}(x)$ and $T_{N2}(x)$ as determined from specific heat ($\blacktriangledown$, $\triangledown$, +), thermal expansion ($\blacktriangle$, $\triangle$, $\times$), DC susceptibility ($\bullet$, $\circ$) and resistivity measurements ($\square$) [9, 18]. Right scale: Kondo-lattice temperature $T^*(x)$, according to Fig. 1 (after scaling lower curve by another factor 1.5).

3.1 Sample preparation and characterization

Ingots of typically $3-5$ g were prepared by melting together Ce (3 N 8), Cu (4 N 9), Ni (4 N 8) and Ge (6 N) in an arc furnace. For compositions $x < 0.05$ and $x > 0.95$, we first prepared master ingots with $x = 0, 0.2, 0.8$ and 1.0 which were subsequently mixed at the appropriate amount and remelted again. This ensures a better homogeneity at low doping level. Characterization by X-ray-powder diffraction and electron-microprobe analysis showed that the samples were single phase, i.e. of the proper $ThCr_2Si_2$ structure, in the whole composition range.

3.2 Bulk measurements

3.2.1 Magnetic susceptibility

The antiferromagnetic ordering of $CeCu_2Ge_2$ at $T_{N1} = 4.1$ K is well documented in the magnetic susceptibility, $\chi(T)$ (top curve of Fig. 3). Low Ni doping ($x \leq 0.2$) results in a continuous depression of $T_{N1}(x)$. Unexpectedly, however, a second anomaly is resolved in the data of the $x = 0.25$ sample and found to shift towards higher temperatures upon increasing the Ni concentration to $x = 0.5$. The latter corresponds to the $T_{N2}(x)$ curve in Fig. 2. A Curie-Weiss-type $\chi(T)$ dependence in the paramagnetic regime exists for all alloys. The apparent flattening of $\chi(T)$ on going from $x \leq 0.5$ to $x \geq 0.75$ corresponds to a pronounced increase in the Kondo-lattice temperature $T^*(x)$ above $x = 0.7$ (see Fig. 1).
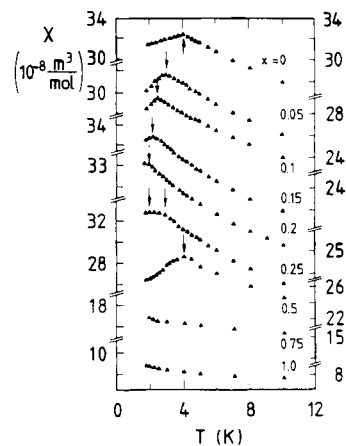
Fig. 3 DC susceptibility χ vs T measured at $B = 1 T$ for $Ce(Cu_{1-x}Ni_x)_2Ge_2$ with different Ni-concentrations, x. Arrows indicate Néel temperatures, cf. Fig. 2.

3.2.2 High-field magnetization

Magnetization measurements on $Ce(Cu_{1-x}Ni_x)_2Ge_2$ compounds were performed at 1.4 and 4.2 K in magnetic fields up to 35 T in the High-Field Installation at the University of Amsterdam [15, 16]. In order to obtain information on the magnetocrystalline aniso-tropy, the measurements were carried out on samples in two forms:

a) powder being free in the sample holder so that it can be oriented by the applied magnetic field, and

b) powder mixed with alcohol and cooled down to liquid-helium temperature in zero magnetic field. In this way, the frozen alcohol fixes the powder in a state of randomly-oriented grains and an ideal polycrystalline sample is simulated.

In Fig. 4, the magnetic isotherms at 1.4 K are shown for free-powder samples of the compounds with x = 0.10, 0.40, 0.55 and 1.00. In the field region below 5 T, the magnetization curves of the compounds with x = 0.10, 0.40 and 0.55 exhibit a slight upward curvature, too small to be visible in Fig. 4. This upward curvature is absent at 4.2 K which indicates that magnetic order sets in below 4.2 K. Above 10 T, the magnetization curves commence to display a tendency to saturate. The magnetization of the compound with x = 1 is perfectly linear up to the highest field measured.
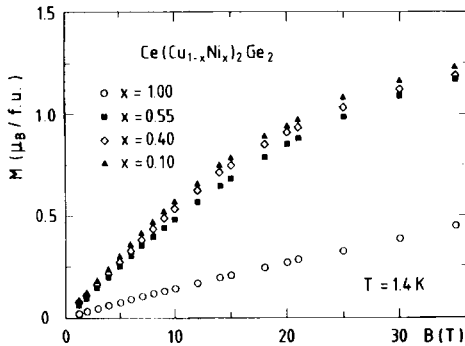

Fig. 4 Magnetization M vs B at T = 1.4 K for x = 0.1, 0.4, 0.55 and 1.0. The results shown were obtained on field-oriented powders, see text.

The magnetic isotherms measured on the fixed-powder samples exhibit the same overall behavior, the magnetization values, however, being lower than those of the free-powder samples, which is indicative of the presence of magnetocrystalline anisotropy in the compounds, see Fig. 5. At 35 T, the values for M_{fix}/M_{free}, the ratio of the magnetizations of the free and fixed powders, amount to 0.82, 0.83 and 0.78 for the compounds with x = 0.10, 0.40, and 0.55, respectively. In the case of uniaxial anisotropy, M_{fix}/M_{free} would have the value of 0.5, whereas higher values correspond to other types of anisotropies. For example, M_{fix}/M_{free} = 0.79 holds for basal-plane anisotropy. Clearly, the anisotropy in the $Ce(Cu_{1-x}Ni_x)_2Ge_2$ compounds is not uniaxial and probably of a more complex type [17]. However, as shown in Fig. 5, the field dependence of M_{fix}/M_{free} for x = 0.10 is different from those for x = 0.40 and 0.55, which suggests the occurence of different types of magnetic order.

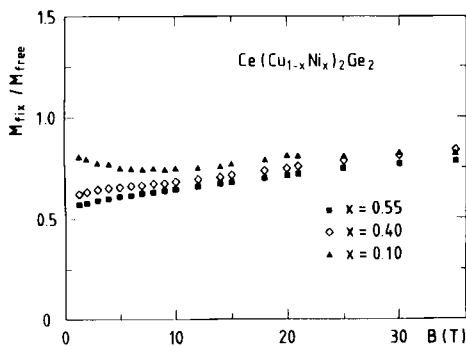**Fig. 5** Ratio of the magnetizations measured at T = 1.4 K for non-oriented and field-oriented powders, M_{fix}/M_{free} vs B, reflecting the magneto-crystalline anisotropy of the magnetically ordered samples with x = 0.1, 0.40 and 0.55.

3.2.3 Specific heat and thermal expansion

Our results of the specific-heat and thermal-expansion measurements on $CeCu_2Ge_2$ and three $Ce(Cu_{1-x}Ni_x)_2Ge_2$ alloys with $x \leq 0.25$ are shown as C/T vs T and a vs T in Figs. 6 and 7. Usually [18] the position of the broad peak in a vs T, found for those alloys with

$x \geq 0.1$, is considered an empirical measure for T^*. The antiferromagnetic ordering temperatures are well documented in both quantities by mean-field-type anomalies. Already for the 2 at% Ni-doped sample one finds two subsequent well-resolved phase transitions. Whereas these are close of merging for $x = 0.1$, their separation increases again on increasing the Ni concentration to $x = 0.25$. The upper transition temperature corresponds to T_{N1} in samples with $x \leq 0.1$ and to T_{N2} for $x \geq 0.2$ (cf. Fig. 2).
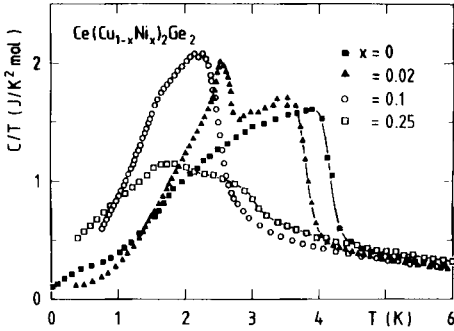

Fig. 6 Specific heat as C/T vs T for Ce(Cu$_{1-x}$Ni$_x$)$_2$Ge$_2$ with $x = 0$ (■), 0.02 (▲), 0.1 (○) and 0.25 (□).
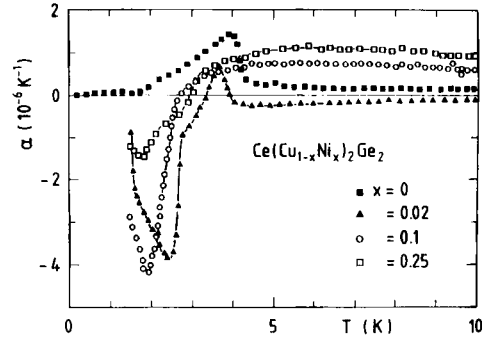
Fig. 7 Coefficient of thermal expansion $\alpha(T)$ vs T for same systems as in Fig. 6.

3.2.4 Electrical resistivity and thermoelectric power

The temperature dependences of these two transport coefficients show rich structure. With the exception of the CeNi$_2$Ge$_2$ compound, all systems exhibit a double-peak behavior in ρ vs $\ln(T/K)$, of which the upper one is ascribed to crystal-field (CF) excitations while the lower one is associated with the onset of coherent scattering at $T \leq T^*$ (Fig. 8). A monotonous, S-shaped $\rho(T)$ dependence is found for the Ni compound ($x = 1$), so as if CF excitations were absent. On the other hand, a CF-derived maximum near $T = 100$ K in the thermoelectric power, S vs $\ln(T/K)$, is not only resolved for samples with $x \leq 0.6$, but exists for $x = 1$ as well (see Fig. 9). It is interesting to note that very similar $\rho(T)$ and $S(T)$ dependences as for CeNi$_2$Ge$_2$ have been reported for the CeRu$_2$Si$_2$ [19, 20], a compound with nearly the same $T^* = 25-30$ K. In particular, the thermopower anomaly characterizing T^* is positive in these two compounds, whereas it is negative for other canonical Ce-based Kondo-lattice systems, e.g. CeAl$_2$ and CeCu$_2$Si$_2$ [20]. Upon replacing more than 40 at% Ni by Cu, however, a negative
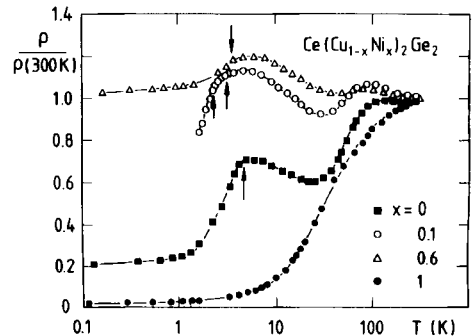

Fig. 8 Resistivity, ρ, vs T on a logarithmic scale for Ce(Cu$_{1-x}$Ni$_x$)$_2$Ge$_2$ with $x = 0, 0.1, 0.6$ and 1. Arrows indicate Néel temperatures, cf. Fig. 2.

extremum near T^* develops and becomes well pronounced for the $CeCu_2Ge_2$ compound, see Fig. 9.

The onset of antiferromagnetic order is indicated in the T-dependences of these two transport coefficients by distinct changes in the slope that coincide with the Néel temperatures derived from the other quantities. Note that the absolute value of the slope of $S(T)$ increases below T_{N1} (e. g. for $x = 0$), but decreases below T_{N2} (e. g. for $x = 0.6$), see Fig. 9.
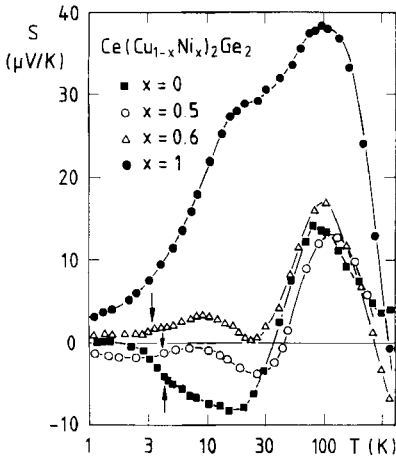

Fig. 9 Thermoelectric power, S vs T on a logarithmic scale for $Ce(Cu_{1-x}Ni_x)_2Ge_2$ with $x = 0$, 0.5, 0.6 and 1. Arrows indicate T_{N1} ($x = 0$) and T_{N2} ($x = 0.5$ and 0.6), respectively.

3.3 Elastic and quasielastic neutron scattering studies

3.3.1 Neutron diffraction

To determine the magnetic structures and the size of the ordered moments, neutron powder-diffraction experiments were performed on the multidetector diffractometer D1B, located on a thermal neutron guide at the HFR of the Institute Laue Langevin (ILL), Grenoble. The wave length of the incident neutrons was 2.55 Å. The magnetic structure of $CeCu_2Ge_2$ had been found earlier [7] to be incommensurate with the chemical cell and was described by a spiral with an ordering wave vector $q_0 = (0.28, 0.28, 0.54)$ in units of $(2\pi/a, 2\pi/c)$ and with a plane of rotation perpendicular to the propagation vector. The ordered moment $\mu_S \simeq 0.74\,\mu_B$ [7] is smaller by a factor of two compared to μ_S expected from the CF ground state. The magnetic diffraction patterns for $x = 0.1$, 0.28, 0.5 and 0.65 are shown in Fig. 10: Here the intensities, as measured in the paramagnetic phase at 6 K, were substracted from the spectra in the magnetically ordered phase at 1.6 K. Like $CeCu_2Ge_2$, the compounds with concentrations $x = 0.1$, 0.28 and 0.5 exhibit a magnetic structure, incommensurate with the chemical lattice. The components of q_0 have been determined using a fit routine to the observed scattering angles. The measured intensities have been compared to calculated values for different modulated structures including spiral and collinear arrangements. The Bragg angles of the magnetic reflections can be indexed in terms of $|Q| = |\tau_{hkl} \pm q_0|$ where (hkl) is a vector of the reciprocal chemical lattice and q_0 is the propagation vector of a modulated spin arrangement.

The difference spectrum for $x = 0.1$ (Fig. 10a) looks similar to that observed in pure $CeCu_2Ge_2$ [7]. The best fit to the measured intensities was obtained for a singleplane spiral, with a plane of rotation perpendicular to the propagation vector $q_0 = (0.28,$

$Ce(Cu_{1-x}Ni_x)_2 Ge_2$ $T = 1.6 K$

Fig. 10 Difference spectra [I(1.6 K) − I(6 K)] for $Ce(Cu_{1-x}Ni_x)_2Ge_2$ with concentrations x = 0.1, 0.28, 0.5 and 0.65: Bragg reflections shown are of magnetic origin only. The positions of the nuclear Bragg reflections are indicated by arrows in (b). For x = 0.1, the (002)$^+$ satellite and for x = 0.28 the (101)$^-$, (101)$^+$ satellites are screened by nuclear Bragg peaks. Specific-heat results for x = 0.65 are given as C/T vs T in the inset of (d).
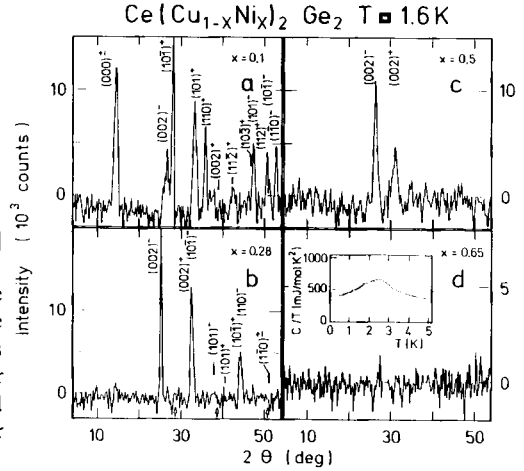
0.28, 0.41). At T = 1.6 K the ordered moment amounts to $\mu_S \approx (0.5 \pm 0.05)\,\mu_S$. For x = 0.28, the pattern of magnetic. Bragg reflections was indexed assuming a longitudinal static spin wave with $\mathbf{q}_0$ = (0.11, 0.11, 0.25) and μ_S = 0.7 $\pm$ 0.2 μ_B (Fig. 10b). Finally, for x = 0.5 two broad magnetic lines show up which are centered symmetrically around the (002) nuclear reflection (Fig. 10c). We identify them as frozen-in incommensurate magnetic correlations along the c axis with a propagation vector $\mathbf{q}_0$ = (0, 0, 0.14). If the intensities of these two satellites are described by a spiral or a static spin wave, an ordered moment of approximately 0.3 μ_B can be deduced. Although the neutron data suggest critical fluctuations, i.e. a correlation length of the same order of magnitude as the modulation length, our bulk measurements indicate long-range magnetic order [9, 21]. The difference spectrum for x = 0.65 reveals no indication of magnetic Bragg reflections (Fig. 10d). Again, long-range magnetic order is inferred from susceptibility and specific-heat measurements, cf. inset of Fig. 10d. From the lack of any magnetic reflections we estimate the ordered moment to be smaller than 0.2 μ_B. Moments of this magnitude cannot be extracted from powder diffraction.

3.3.2 Quasielastic neutron scattering

Quasielastic neutron-scattering experiments are an ideal tool to study the temperature and the wave-vector dependence of the magnetic relaxation rate. In addition, a careful analysis of the lineshapes of the quasielastic scattered intensities may allow to characterize the origin of the magnetic relaxation as being due to either on-site or inter-site correlations [22]. Measurements of the quasielastic line width were performed at the time-of-flight spectrometer IN6 located at a cold source of the HFR at the ILL. Incident energies of 3.15 meV were used, and $Ce(Cu_{1-x}Ni_x)_2Ge_2$ compounds with concentrations x = 0, 0.28, 0.5, 0.65 and 1 were investigated at temperatures 1.5 K < T < 200 K. Fig. 11 shows the quasielastic line for x = 0.5 as function of temperature. At all temperatures, even in the magnetically ordered phase, the neutron intensities are well described by a broad Lorentzian line (solid line), in addition to the narrow elastic incoherent line. $S(\mathbf{Q}, \omega)$ is purely quasielastic for $T > T_{N2}$. At T = 1.5 K, in the magnetically ordered phase, the center of the Lorentzian line is shifted to 0.6 meV corresponding to an average magnetic excitation energy. Fig. 12 shows the quasielastic line in the paramagnetic phase ($T \approx 5$ K) for x = 0, 0.28, 0.65 and 1. For x = 0, strong deviations form the Lorentzian

line shape [7] indicate the existence of inter-site spin correlations. For $x \geq 0.28$ the quasielastic line shape closely follows a Lorentzian behavior. The Kondo-lattice temperature, as read off the residual quasielastic line width is plotted in Fig. 1 and compared to T^* as determined from maxima in the temperature dependences of the thermal expansion, resistivity and thermopower, respectively. The increase of the $4f$-conduction electron hybridization with increasing concentration is well documented by the increase of the line width. The temperature dependence of the magnetic relaxation rate for $x = 0.28$, 0.5 and 0.65, as determined from the line width Γ (half width at half maximum) of the quasielastic line, is shown in Fig. 13.
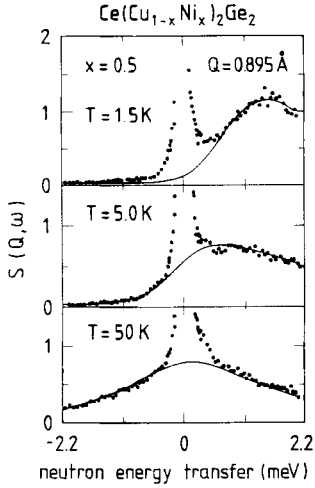

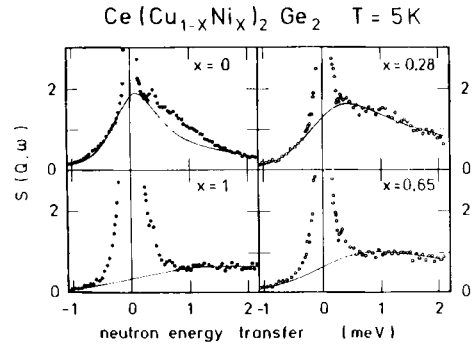Fig. 11 Temperature dependence of scattering law vs neutron-energy transfer at fixed $Q = 0.895$ Å^{-1} for Ce(Cu$_{0.5}$Ni$_{0.5}$)$_2$Ge$_2$.

Fig. 12 Scattering law vs neutron-energy transfer for an average scattering angle $\theta = 19$ deg as obtained in Ce(Cu$_{1-x}$Ni$_x$)$_2$Ge$_2$ for concentrations $x = 0$, 0.28, 0.65 and 1 at $T = 5$ K. Solid lines are the results of fits using a Lorentzian line shape. Data for $x = 0$, and $x = 1$ are taken from [7] and [8], respectively.
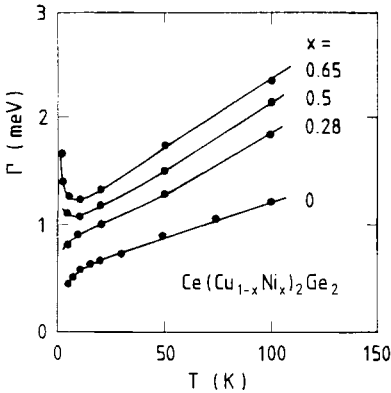

Fig. 13 Magnetic relaxation rate Γ (HWHM) vs temperature for Ce(Cu$_{1-x}$Ni$_x$)$_2$Ge$_2$ with $x = 0$, 0.28, 0.5 and 0.65.

4. Discussion

In the following we wish to provide evidence that the two types of antiferromagnetic phases in Ce(Cu$_{1-x}$Ni$_x$)$_2$Ge$_2$ correspond to LMM and HFBM, respectively. Strong support for this interpretation comes from the neutron-scattering results and from a comparison of the experimentally determined T-x-phase diagram with theoretical predictions [3, 11].

The short propagation vector and the small ordered moment found for the $x = 0.5$ sample, characterize a modulated spin arrangement which extends over almost ten lattice constants and thus fully meets the theoretical prediction of HFBM. In addition, the gradual reduction of the saturation moment upon increasing Ni concentration suggests that the transition from a local-moment to a band-like magnetic state is a gradual one. A crucial test for the validity of the physical picture proposed above certainly lies in the application of the theory to the complete phase diagram of the $Ce(Cu_{1-x}Ni_x)_2Ge_2$ system. Evaluation of the susceptibility (Eq. 1) on the basis of *LNCA* theory for an Anderson-type lattice model, using a tight-binding band of realistic tetragonal crystal symmetry, bandwidth and degree of anisotropy, furnishes phase-transition lines in a coupling constant vs. temperature diagram [11]. Whereas the susceptibility, evaluated in the whole Brillouin zone, exhibits a rather rich structure, characterized by peaks at short (as indicative for hybridization gaps and thus for HFBM) and at larger wave vectors (typically of the order of a diameter of the Fermi surface as indicative for RKKY correlations), we have chosen the most unstable mode only to be connected with an instability, i.e. we have looked for the first zero occuring in the denominator of $\chi(\mathbf{q}, o)$. Additionally, an average over the direction of $\mathbf{q}$ was taken to simplify calculations and to simulate measurements on powders. The results are shown in Fig. 14: T^* markes the

Fig. 14 Comparison between theoretical [11] (solid curves) and experimental results for three selected $Ce(Cu_{1-x}Ni_x)_2Ge_2$ samples ($x = 0$, 0.5 and 0.75). Same symbols as in Figs. 1 and 2. Temperatures are normalized by the Anderson width ($\Delta = \pi N_F V^2$); g is the microscopic coupling constant. Dashed lines indicate experimental results for $T_{N1}(x)$ and $T_{N2}(x)$, $x < 0.5$, cf. Fig. 2.
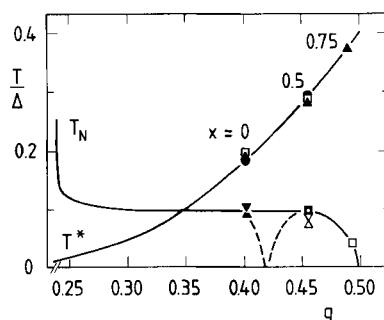
calculated Kondo-lattice temperature and T_N the temperature of the magnetic instability. The character of the magnetic state changes continuously from RKKY type (LMM) at smaller g to *HFBM* at larger g, the crossover occuring between $g = 0.3$ and $g = 0.45$ where T_N and T^* intersect. In this region of intermediate g the true magnetic state could be influenced by a competition of both types of order and by anisotropy effects. Thus we cannot expect the simple theoretical procedure of extracting the phase transition from the dominating instability of the susceptibility to be correct here. The experimental phase transition lines contained in Fig. 1 can be compared to these theoretical predictions via the following procedure: The experimental ratio T^*/T_N which is about 3 for $x = 0.5$, is found in the theoretical results at $g = 0.45$. We identify these points in the two phase diagrams and thereby also gauge the theoretical temperature axis in Kelvin units. Assuming a linear dependence between coupling constant g and Ni-composition x there is only one second free parameter to fix the proportion of g and x. Surprisingly then, all experimental values for T^* and T_N in the HFBM region $g \geq 0.45$ fall on the respective theoretical curve. In the left hand side of the phase diagram agreement is not so good. In particular, we ascribe the deviation indicated by the dashed lines to the magnetic competition effects mentioned above. The main source of the discrepancy, however, can be assigned to a non-linear connection between composition

and coupling constant. In fact, an overall linear dependence between hybridization intensity $V^2 \sim g$ and composition would seem fortuitous. In summary, we take the good agreement between theory and experiment, which also entails the consistent characterization of the magnetic phases, as a strong support for HFBM.

Further support for our interpretation in terms of an alloying-induced transition from LMM to HFBM results from the analysis of the quasielastic line shapes (Fig. 2). Interactions of the $4f$ moment with the conduction electrons introduce relaxation effects and result in a Lorentzian broadening of the quasielastic scattering intensity. Deviations from the Lorentzian line shape can be associated with critical spin fluctuations due to inter-site interactions [22]. In fact, theory predicts a Lorentzian line shape with a line width slightly larger than T^*, which essentially results from quasi-local processes only, in the heavy Fermi liquid, whereas non-Lorentzian contributions are present at smaller g due to the release of RKKY-type fluctuations [11]. As stated previously, for $x \geq 0.28$ the quasielastic line shape follows a Lorentzian behavior (Fig. 12). This observation supports our interpretation that the antiferromagnetic order of the HFBM develops out of a heavy Fermi liquid.

Remarkable differences between the weakly and strongly Ni-doped systems, i.e. between LMM and HFBM, are also found in the results of our magnetization and thermopower measurements. The field dependence of the ratio M_{fix}/M_{free} for $x = 0.10$ displays an initial decrease (up to about 7 Tesla), which can be understood in terms of LMM in a Kondo system (Fig. 5) in which the ordered moments are reduced due to the formation of a Kondo singlet: A sufficiently strong external field reduces the Kondo screening and, thus, the local $4f$ moment is gradually recovered. This effect will contribute mainly to the magnetization in the easy directions. On the other hand, for $x = 0.4$ and 0.55 the ratios M_{fix}/M_{free} are monotonously increasing (Fig. 5). Apparently, effects associated with the Kondo compensation of local moments as observed for $x = 0.1$ are absent for $x \geq 0.4$. In addition, as is seen in Fig. 9, the marked change of the absolute slope in the temperature dependence of the thermopower at the onset of antiferromagnetic order is positive for cooling through $T = T_{N1}$ ($x = 0.1$), while it is negative at $T = T_{N2}$ ($x = 0.5$ and 0.6). No significant difference in the respective resistivity curves $\rho(T)$ can, however, be resolved (Fig. 8). This demonstrates the well known fact that thermopower responds more sensitively to changes in the electronic structure at E_F than electrical resistivity does.

Finally we wish to briefly mention several experimental observations which seem to be less directly connected to the LMM-HFBM transition:

(1) Our specific-heat results of which only those on Ni-poor samples are shown in Fig. 6, yield the concentration dependence of the entropy, $\mathscr{S}(x)$. Taken at $T = 5$ K, $\mathscr{S}(x)$ is found to decrease almost linearly with increasing Ni concentration. This behavior is in accord with the smooth increase of the Kondo-lattice temperature $T^*(x)$ for $x < 0.7$. However, $\mathscr{S}(x)$ does *not* reflect the marked rise in $T^*(x)$ for higher x (Fig. 1): For a doublet ground state, broadened by Kondo interactions, an additional increase in $T^*(x)$ should result in an additional reduction of the entropy $\mathscr{S}(x)$ when measured at a fixed temperature $T < T^*$. We believe that this reduction is compensated by an increasing admixture of excited CF states to the doublet ground state. Our view is corroborated by the concentration dependence of $\Gamma(T)$, the quasielastic line width (Fig. 13). For $x \leq 0.28$, the magnetic relaxation rate exhibits a monotonous increase upon heating. However, a minimum in $\Gamma(T)$ appears for $x \geq 0.5$. According to Ref. 23, this remarkable observation suggests a groundstate degeneracy $N > 2$. For $CeNi_2Ge_2$ no evidence for CF excitations could be found in inelastic neutron-scattering experiments [8] and in the temperature

dependence of the resistivity (Fig. 8). Since, on the other hand, the temperature dependence of the thermopower exhibits a pronounced CF-derived peak near $T = 100$ K in the *whole* concentration range $0 \leq x \leq 1$, we conclude that the phenomena listed above originate in a large broadening of the excited CF states triggered by the strongly increasing Kondo interaction for $x > 0.7$.

(2) The Néel temperature $T_{N1}(x)$ is precipitously depressed with increasing Ni concentration $x < 0.2$ (Fig. 2). If this drop were dominated by a volume compression, one would expect $CeCu_2Ge_2$ to exhibit a Néel temperature with negative pressure coefficient. According to Ehrenfest's relation

$$t_p = \frac{1}{T_N} \left(\frac{\delta T_N}{\delta p_h} \right)_{P_h \to 0} = 3 V_{mol} \frac{\Delta a}{\Delta C_p} \tag{2}$$

a negative jump in the thermal-expansion coefficient, Δa_1, should be observed at $T_{N1} = 4.1$ K, in view of the positive specific-heat jump, ΔC_p (Fig. 5). However, Δa_1 is found to be positive not only for the undoped compound, but also for the alloy containing 2 at% Ni. This clearly shows that the actual depression of $T_{N1}(x)$ cannot be dominated by the Ni-induced compression of the volume. Presumably, band-structure effects are more important, since for the Ni dopant the $3d$ states are close to E_F, whereas they lie way below E_F for Cu.

(3) Two phase-transition anomalies are well resolved in the temperature dependences of both the specific heat (Fig. 15a) and the susceptibility (Fig. 15b) of $Ce(Cu_{1-x}Ni_x)_2$ systems with $0 < x \leq 0.3$. For $x = 0.25$, the upper transition temperature is identified with T_{N2}, while the lower one had been tentatively ascribed [4] to a superposition of the incommensurate "short-q_0" spin structure with a second one, perhaps the one that is identified for the Ni-poor alloys. One possibility is that the two different structures ascribed before to LMM and HFBM coexist on different, almost disjunct portions of the (renormalized) Fermi surface.

Fig. 15 Double phase transitions in $Ce(Cu_{0.75}Ni_{0.25})_2Ge_2$. (a) Specific heat as C/T vs T. Measured curve can be decomposed into two bulk phase-transition anomalies as indicated by solid lines. (b) DC susceptibility, χ vs T measured at $B = 50$ mT and 1 T, respectively (arrows indicate two different antiferromagnetic transitions, cf. Fig. 2).
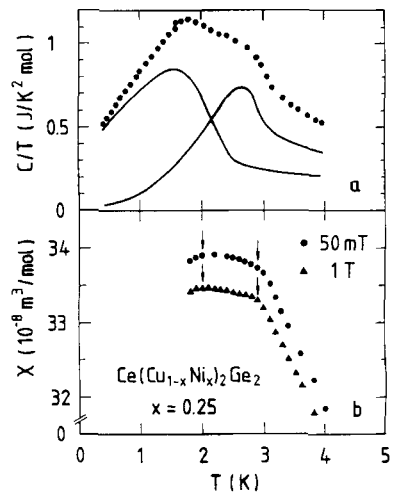
5 Conclusion

The magnetic phase diagram of $Ce(Cu_{1-x}Ni_x)_2Ge_2$, spanning from local-moment based antiferromagnetic ordering at low ($x \leq 0.2$) to a HF phase at high ($x > 0.75$) Ni concentrations, exhibits in the intermediate composition range ($0.5 < x < 0.75$) a new type of antiferromagnetism that is characterized by (i) a substantially reduced ordered moment, (ii) a short modulation wave vector in full agreement with theoretical predictions [3, 11] and (iii) a magnetic neutron-scattering cross section dominated by single-site relaxation effects. We ascribe this phase to "band magnetism" in the system of strongly renormalized quasiparticles. The transition from a local-moment to this itinerant-type of antiferromagnetism is reflected by distinct changes in both the field dependence of the magnetization and the temperature dependence of the thermopower.

References

[1] For reviews, see: G. R. Stewart, Rev. Mod. Phys. **56** (1984) 755; C. M. Varma, Comments on Solid State Phys. **11** (1985) 221; F. Steglich, Springer Series in Solid-State Sciences **62** (1985) 23; P. A. Lee, T. M. Rice, J. W. Serene, L. J. Sham, J. W. Wilkins, Comments on Condensed Matter Phys. **12** (1986) 99; H. R. Ott, Progr. Low Temp. Phys. **XI** (1987) 215; P. Fulde, J. Keller, G. Zwicknagl, Solid State Phys. **41** (1988) 1

[2] N. Grewe, Th. Pruschke, Z. Physik B **60** (1985) 311; N. Grewe, Th. Pruschke, H. Keiter, Z. Physik B **71** (1988) 75

[3] N. Grewe, B. Welslau, Solid State Commun. **65** (1988) 437

[4] F. Steglich, G. Sparn, R. Moog, S. Horn, A. Grauel, M. Lang, M. Novak, A. Loidl, A. Krimmel, K. Knorr, A. P. Murani, M. Tachiki, Physica B **163** (1990) 19; F. Steglich, C. Geibel, S. Horn, U. Ahlheim, M.Lang, G. Sparn, A. Loidl, A. Krimmel, W. Assmus, J. Mag. Mag. Mater **90, 91** (1990) 383

[5] N. Grewe, F. Steglich, in: Handbook on the Physics and Chemistry of Rare Earths, Vol. 14, K. A. Gschneidner, Jr., L. Eyring (eds. North-Holland, Amsterdam) 1991, p. 343

[6] F. R. de Boer, J. C. P. Klaasse, P. A. Veenhuizen, A. Böhm, C. D. Bredl, U. Gottwick, H. M. Mayer, L. Pawlak, U. Rauchschwalbe, H. Spille, F. Steglich, J. Magn. Magn. Mat. **63, 64** (1987) 91

[7] G. Knopp, A. Loidl, K. Knorr, L. Pawlak, M. Duczmal, R. Caspary, U. Gottwick, H. Spille, F. Steglich, A. P. Murani, Z. Phys. B **77** (1989) 95; G. Knopp, Dissertation, University of Mainz 1989, unpublished

[8] G. Knopp, A. Loidl, R. Caspary, U. Gottwick, C. D. Bredl, H. Spille, F. Steglich, A. P. Murani, J. Magn. Magn. Mat. **74** (1988) 341

[9] A. Böhm, R. Caspary, U. Habel, L. Pawlak, A. Zuber, F. Steglich, A. Loidl, J. Magn. Magn. Mat. **76, 77** (1988) 150; D. Enkler, Diploma Thesis, TH Darmstadt 1989, unpublished; M. Nowak, Diploma Thesis, TH Darmstadt 1989, unpublished; A. Grauel, Diploma Thesis, TH Darmstadt 1989, unpublished; W. Denz, Diploma Thesis, TH Darmstadt 1989, unpublished

[10] S. Doniach, Physica B **91** (1977) 231

[11] B. Welslau, N. Grewe, Physica B **165, 166** (1990) 387

[12] Y. Kuramoto, Physica B **156, 157** (1989) 789

[13] Y. Kuramoto, K. Miyake, J. Phys. Soc. Jpn. **59** (1990) 2831

[14] P. Fazekas, E. Müller-Hartmann, Z. Phys. B **85** (1991) 285

[15] R. Gersdorf, F. R. de Boer, J. C. Wolfrat, F. A. Muller, L. W. Roeland, in: High Field Magnetism, M. Date (ed. North-Holland, Amsterdam) 1983, p. 277

[16] L. W. Roeland, R. Gersdorf, W. C. M. Mattens, Physica B **155** (1989) 58

[17] V. Sechovsky, L. Havela, in: Ferromagnetic materials, E. P. Wohlfarth, K. H. J. Buschow (eds. North-Holland, Amsterdam) 1988, p. 324

[18] R. Schefzyk, J. Heibel, F. Steglich, R. Felten, G. Weber, J. Magn. Magn. Mat. **47, 48** (1985) 83

[19] L. C. Gupta, D. E. MacLaughlin, Cheng Tien, C. Godart, M. A. Edwards, R. D. Parks, Phys. Rev. B **28** (1983) 3673

[20] F. Steglich, U. Rauchschwalbe, U. Gottwick, H. M. Mayer, G. Sparn, N. Grewe, U. Poppe, J. J. M. Franse, J. Appl. Phys. **57** (1985) 3054

[21] G. Sparn, R. Caspary, U. Gottwick, A. Grauel, U. Habel, M. Lang, M. Novak, R. Schefzyk, W. Schiebeling, H. Spille, M. Winkelmann, A. Zuber, F. Steglich, A. Loidl, J. Magn. Magn. Mat. **76, 77** (1988) 153

[22] U. Walter, M. Loewenhaupt, E. Holland-Moritz, W. Schlabitz, Phys. Rev. B **36** (1987) 1981

[23] N. E. Bickers, D. L. Cox, J. W. Wilkins, Phys. Rev. Lett. **54** (1985) 230